1,2-dibromoethane (50 μL, 0.58 mmol). After addition of 3 g of DCPD (15 mmol) the mixture was warmed on a water bath to slight reflux, and cyclopropyl bromide (0.4 mL, 5 mmol) was added all at once. The reaction started within 5 min, and the cyclopropane was trapped as previously described. The yield was determined by ^{1}H NMR spectroscopy to be 1.34 mmol (26%), of which 15% was cyclopropane-d_1 and 85% cyclopropane-d_0.

The remaining solution was cooled to 0 °C, and 2 mL of methanol was added. The cyclopropane was trapped in a second cooling trap. The yield of cyclopropane was determined to be 0.33 mmol (6%).

Preparation and Solid-State Structural, Electronic, and Magnetic Properties of the 1,3,5-Benzene-Bridged Tris(1,2,3,5-dithiadiazolyl) [1,3,5-$C_6H_3(CN_2S_2)_3$]

A. W. Cordes,*[1a] R. C. Haddon,*[1b] R. G. Hicks,[1c] R. T. Oakley,*[1c] T. T. M. Palstra,[1b] L. F. Schneemeyer,[1b] and J. V. Waszczak[1b]

Contribution from the Department of Chemistry and Biochemistry, University of Arkansas, Fayetteville, Arkansas 72701, AT&T Bell Laboratories, Murray Hill, New Jersey 07974, and Guelph Waterloo Centre for Graduate Work in Chemistry, Guelph Campus, Department of Chemistry and Biochemistry, University of Guelph, Guelph, Ontario N1G 2W1, Canada.
Received December 17, 1991

Abstract: The preparation and solid-state characterization of the trifunctional radical 1,3,5-benzenetris(1,2,3,5-dithiadiazolyl) [4,4′,4″-(1,3,5-benzenetriyl)tris[1,2,3,5-dithiadiazolyl], 1,3,5-$C_6H_3(CN_2S_2)_3$] are described. The crystals belong to the monoclinic space group $P2_1/c$, with a = 6.927 (2), b = 19.798 (3), c = 19.393 (3), and β = 99.80 (2) Å^3. The crystal structure consists of stacks of triradicals running parallel to x. Each radical center associates with a neighboring radical, generating alternating long (mean 3.832 Å) and short (mean 3.117 Å) interradical S···S contacts along the stack; only two of the three crystallographically distinct bond alternation waves so generated are in-phase. The packing of triradical stacks produces an extensive network of close interstack S···S contacts. The compound is diamagnetic at room temperature, but paramagnetic defects begin to appear near 450 K. The room-temperature single-crystal conductivity is near 10^{-7} S cm^{-1}. Extended Hückel band structure calculations reveal a band gap of 0.8 eV.

Introduction

Our interest in the design of molecular conductors based on neutral[2] as opposed to charged radicals has focused on the use of heterocyclic 1,2,3,5-dithiadiazolyl and 1,2,3,5-diselenadiazolyl systems **1**.[3] The basic architectural strategy we have pursued involves the design of molecular "building blocks" which, in the solid state, adopt stacked structures, e.g., **2**, with strong intra- and interstack interactions. We have demonstrated that stacking of monofunctional radical dimers can be induced by the use of cyanoaryl[4] or cyanofuryl[5] substituents, but the long-range E···E (E = S, Se) contacts between and within the dimer stacks are generally weak. Tighter structures, with better conductivity characteristics, can be generated from bifunctional radicals, such as the 1,4- and 1,3-phenylene bridged systems **3** and **4**, respectively. Molecular stacks, however, are not always found; indeed the crystal structure of the 1,4-derivatives (E = S and Se) consists of dimers packed in a herringbone-like fashion.[6] Stacks of diradical units, linked vertically through alternate ends, are observed in the α-phase of 1,3-derivatives (E = S and Se),[7] but in the β-phase of

Scheme I

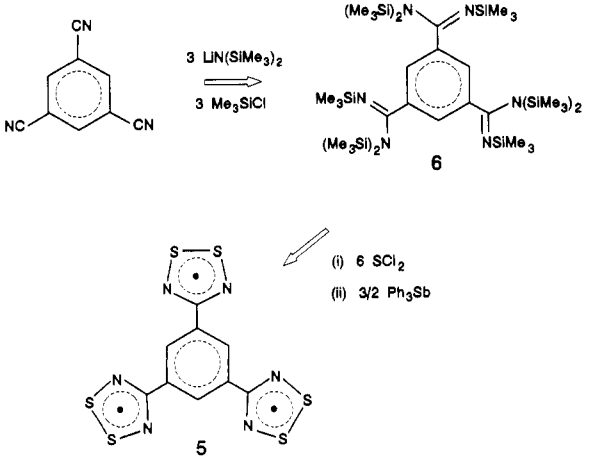

4 (E = Se) the radicals associate as dimers which coil together to generate a chainlike motif.[8]

As an extension of this work, we have prepared and characterized the trifunctional radical 1,3,5-benzenetris(1,2,3,5-dithiadiazolyl) [4,4′,4″-(1,3,5-benzenetriyl)tris[1,2,3,5-dithiadiazolyl],

(1) (a) University of Arkansas. (b) AT&T Bell Laboratories. (c) University of Guelph.
(2) (a) Haddon, R. C. *Aust. J. Chem.* **1975**, *28*, 2343. (b) Haddon, R. C. *Nature (London)* **1975**, *256*, 394.
(3) Cordes, A. W.; Haddon, R. C.; Oakley, R. T. In *The Chemistry of Inorganic Ring Systems*; Steudel, R., Ed.; Elsevier: Amsterdam, 1992; p 295.
(4) Cordes, A. W.; Haddon, R. C.; Hicks, R. G.; Oakley, R. T.; Palstra, T. T. M. *Inorg. Chem.* in press.
(5) Cordes, A. W.; Chamchoumis, C. M.; Hicks, R. G.; Oakley, R. T.; Young, K. M.; Haddon, R. C. *Can. J. Chem.*, in press.
(6) Cordes, A. W.; Haddon, R. C.; Oakley, R. T.; Schneemeyer, L. F.; Waszczak, J. V.; Young, K. M. *Zimmerman, N. M. J. Am. Chem. Soc.* **1991**, *113*, 582.
(7) Andrews, M. P.; Cordes, A. W.; Douglass, D. C.; Fleming, R. M.; Glarum, S. H.; Haddon, R. C.; Marsh, P.; Oakley, R. T.; Palstra, T. T. M.; Schneemeyer, L. F.; Trucks, G. W.; Tycko, R.; Waszczak, J. V.; Young, K. M.; Zimmerman, N. M. *J. Am. Chem. Soc.* **1991**, *113*, 3559.
(8) (a) Cordes, A. W.; Haddon, R. C.; Hicks, R. G.; Oakley, R. T.; Palstra, T. T. M.; Schneemeyer, L. F.; Waszczak, J. V. *J. Am. Chem. Soc.* **1992**, *114*, 1729.

0002-7863/92/1514-5000$03.00/0

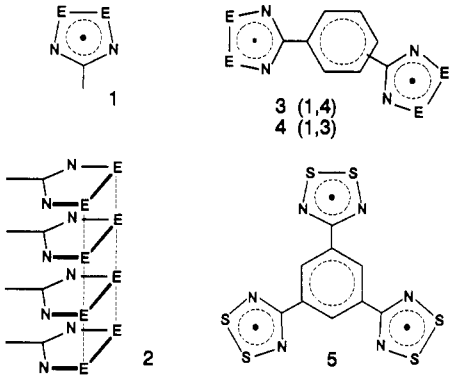

5]. Herein we report the crystal structure and solid-state properties of this material. The results are discussed in the light of extended Hückel band structure calculations.

Results

Synthesis. The preparative route to **5** (Scheme I) is analogous to that used for other monofunctional and bifunctional radicals.[6,7,9] The necessary starting material, 1,3,5-benzenetris[*N*,*N*,*N*′-tris(trimethylsilyl)carboxamidine] (**6**), can be made by treatment of 1,3,5-tricyanobenzene with 3 equiv of lithium bis(trimethylsilyl)amide, followed by transmetalation with trimethylsilyl chloride. Reaction of the tris-amidine with 6 molar equiv of SCl_2 affords the tris(1,2,3,5-dithiadiazolium) trication as its trichloride salt. Reduction of the trication with triphenylantimony affords **5** as a black powder, which is completely insoluble in all organic media. The material can, however, be purified by high vacuum sublimation at 270 °C/10^{-2} Torr to yield small metallic grey needles. Attempts to make the corresponding selenium derivative have been unsuccessful; although a similar synthetic sequence (using selenium dichloride and **6**) can be carried through in a fashion analogous to that described for **5**, attempts to purify the product by vacuum sublimation have been thwarted by its extreme involatility.

Crystal Structure. Crystals of **5** belong to the monoclinic space group $P2_1/c$; atom coordinates are provided in Table I. All internal bond lengths and angles are normal (see Table II). An ORTEP drawing of the asymmetric unit, giving the atom numbering scheme, is shown in Figure 1.

The crystal structure consists of stacks of triradicals running parallel to the x axis. The unit cell (Figure 2) contains four such stacks packed together in a pseudo-pinwheel fashion similar to that observed in the α-phase of **4**. The lattice symmetry distinguishes between the three radical rings in each triradical unit, thus affording the three columns labeled A, B, and C (Figures 2 and 3). As can be seen in Figure 3, which illustrates the construction of a triradical column, the three radical stacks associate to form sequences of alternating long and short interradical S···S contacts (see Table III). The phase of this bond alternation in the B stack is opposite that observed in the A and C stacks, i.e., a more complex version of the zigzag alternation pattern observed in α-**4**. Despite the distortion from regularly spaced radical centers, the benzene rings remain evenly spaced; the two distinct centroid-to-centroid distances are 3.460 and 3.493 Å.

In addition to the close S···S contacts within the radical stacks, there are numerous interactions between adjacent stacks, arising, most notably, from the pinwheellike approaches of the B and C stacks about the inversion centers at, for example, $x/2$, $y/2$, $z/2$, and the head-on approach of A stacks about inversion centers at, for example, $x/2$, $y/2$, 0. Figures 4 and 5 illustrate the nature of these interstack contacts, whose values are defined in Table II. In the case of the BC cluster, the sulfur atoms shown in Figure 4 are the innermost of each radical ring. The phase properties of the four bond alternation waves are defined by the inversion centers. The origin of the four close contacts associated with each atom within the cluster can be appreciated by reference to the

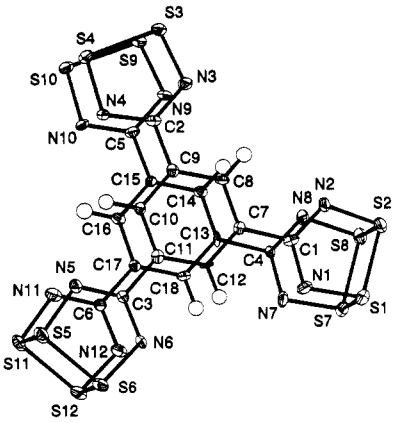

Figure 1. ORTEP drawing of the asymmetric unit in **5**, showing atom numbering scheme.

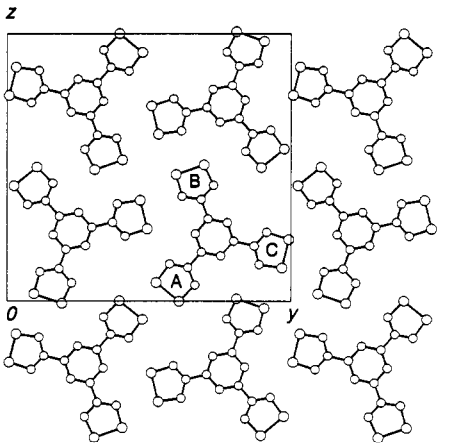

Figure 2. Projection of the cell packing of **5** in the yz plane. The three distinct CN_2S_2 rings are designated A, B, and C.

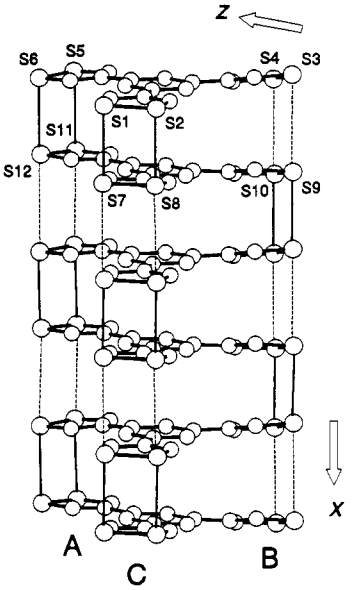

Figure 3. Single column of triradicals, showing the association of A, B, and C stacks. Short and long intrastack contacts are defined in Table III.

idealized arrangement shown in Figure 4. One of the contacts listed in Table II, namely S1···S4″, which lies opposite the very short S1···S4′ contact, is well outside the van der Waals range[10] and is included only for completeness. In addition to these interactions, there is a moderately short (3.895 (3) Å) contact

(9) Del Bel Belluz, P.; Cordes, A. W.; Kristof, E. M.; Kristof, P. V.; Liblong, S. W.; Oakley, R. T. *J. Am. Chem. Soc.* **1989**, *111*, 9276.

(10) Bondi, A. *J. Phys. Chem.* **1964**, *68*, 441.

Table I. Atomic Coordinates for 1,3,5-$[C_6H_3(CN_2S_2)_3]$ (**5**)[a]

	x	y	z	B_{iso}[b]
S1	0.4697 (3)	0.98164 (10)	0.12692 (11)	2.45 (9)
S2	0.5020 (3)	1.00605 (10)	0.23270 (11)	2.57 (9)
S3	0.8231 (3)	0.70255 (10)	0.50825 (10)	2.44 (9)
S4	0.7798 (3)	0.60470 (10)	0.47047 (11)	2.36 (8)
S5	0.6404 (3)	0.54041 (10)	0.06573 (11)	2.57 (9)
S6	0.5693 (4)	0.62125 (11)	−0.00390 (11)	2.81 (10)
S7	0.0183 (3)	0.96783 (10)	0.12425 (11)	2.40 (8)
S8	0.0545 (3)	0.99233 (10)	0.23018 (11)	2.76 (10)
S9	0.2628 (3)	0.69294 (10)	0.50888 (10)	2.34 (9)
S10	0.2323 (3)	0.59441 (10)	0.47246 (10)	2.29 (9)
S11	0.1825 (3)	0.52413 (10)	0.06947 (11)	2.51 (9)
S12	0.1282 (3)	0.60500 (11)	−0.00126 (11)	2.71 (9)
N1	0.5155 (10)	0.9020 (3)	0.1395 (3)	2.3 (3)
N2	0.5566 (10)	0.9294 (3)	0.2601 (3)	2.2 (3)
N3	0.7718 (10)	0.7385 (3)	0.4313 (3)	2.3 (3)
N4	0.7270 (10)	0.6277 (3)	0.3876 (3)	2.1 (3)
N5	0.6648 (10)	0.5872 (3)	0.1365 (3)	2.1 (3)
N6	0.5832 (11)	0.6772 (3)	0.0582 (3)	2.3 (3)
N7	0.0476 (9)	0.8871 (3)	0.1374 (3)	2.2 (3)
N8	0.0874 (10)	0.9143 (3)	0.2570 (3)	2.2 (3)
N9	0.2384 (10)	0.7269 (3)	0.4319 (3)	2.1 (3)
N10	0.1972 (10)	0.6154 (3)	0.3902 (3)	2.0 (3)
N11	0.1916 (10)	0.5715 (3)	0.1393 (3)	2.3 (3)
N12	0.1277 (10)	0.6608 (3)	0.0603 (3)	2.2 (3)
C1	0.5568 (10)	0.8841 (4)	0.2078 (4)	1.6 (3)
C2	0.7312 (11)	0.6949 (4)	0.3786 (4)	1.7 (3)
C3	0.6318 (11)	0.6523 (4)	0.1227 (4)	1.7 (3)
C4	0.0801 (11)	0.8700 (3)	0.2058 (4)	1.5 (3)
C5	0.2026 (11)	0.6823 (4)	0.3787 (4)	1.8 (3)
C6	0.1578 (11)	0.6357 (4)	0.1255 (4)	1.5 (3)
C7	0.6064 (10)	0.8125 (3)	0.2243 (4)	1.5 (3)
C8	0.6456 (11)	0.7889 (4)	0.2932 (4)	1.6 (3)
C9	0.6868 (11)	0.7211 (3)	0.3057 (4)	1.7 (3)
C10	0.6844 (10)	0.6762 (3)	0.2511 (4)	1.5 (3)
C11	0.6434 (10)	0.7000 (4)	0.1818 (4)	1.5 (3)
C12	0.6054 (10)	0.7676 (3)	0.1701 (3)	1.4 (3)
C13	0.1145 (10)	0.7973 (3)	0.2238 (4)	1.5 (3)
C14	0.1427 (11)	0.7752 (4)	0.2916 (4)	1.6 (3)
C15	0.1763 (10)	0.7071 (3)	0.3062 (4)	1.4 (3)
C16	0.1810 (10)	0.6615 (4)	0.2526 (4)	1.5 (3)
C17	0.1529 (10)	0.6834 (3)	0.1838 (4)	1.3 (3)
C18	0.1193 (10)	0.7513 (3)	0.1698 (3)	1.4 (3)
H8	0.643	0.820	0.331	2.4
H10	0.709	0.629	0.259	2.2
H12	0.577	0.785	0.124	2.2
H14	0.138	0.807	0.329	2.4
H16	0.206	0.615	0.262	2.4
H18	0.098	0.767	0.123	2.3

[a] esd's (in parentheses) refer to the last digit printed. [b] B_{iso} is the mean of the principal axes of the thermal ellipsoid.

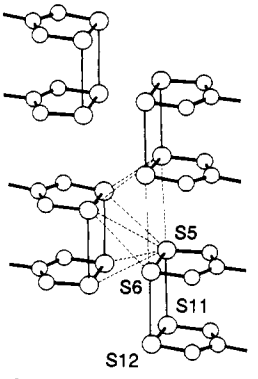

Figure 4. Interstack S···S interactions arising from the head-on approach of two A stacks. The contacts shown with dashed lines are defined in Table III.

between S6 on ring A and S3 on ring B.

Magnetic and Conductivity Measurements. The measured magnetic susceptibility of **5** as a function of temperature is shown in Figure 6. As observed in both **3** and **4** (E = S), the low-temperature regime shows Curie behavior, consistent with the

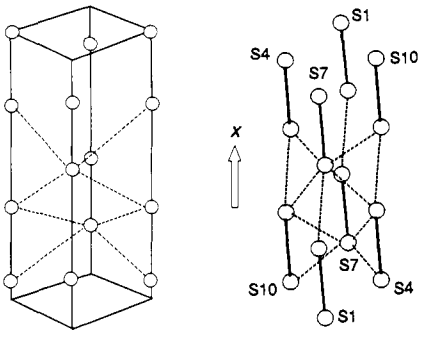

Figure 5. Interstack S···S interactions arising from the pinwheellike approach of pairs of B and C stacks. Only the innermost sulfur on each CN_2S_2 ring is shown. The drawing (left) provides an idealized view of the actual packing (right). The contacts shown with dashed lines are defined in Table III.

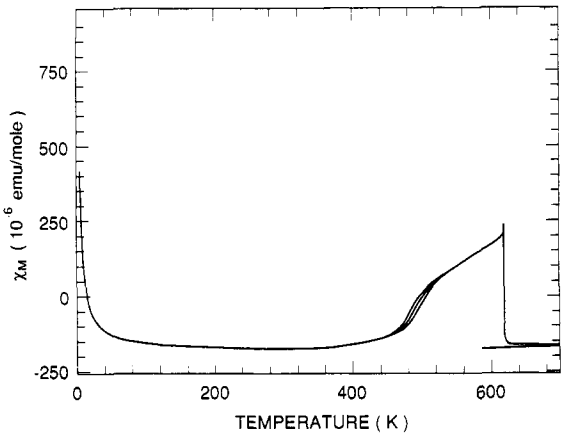

Figure 6. Magnetic susceptibility of **5** as a function of temperature.

presence of low levels of paramagnetic defects arising from unpaired radicals. The concentration of defects obtained from a Curie–Weiss fit to the data in Figure 6 was 1.0% on a per molecule basis, which is similar to the values found for **4** (0.97%). The θ value was 4 K, and the measured diamagnetism was −192 ppm emu mol^{-1}.

The magnetism of **5** begins to rise slowly above 400 K and more rapidly above 450 K, following a pattern reminiscent of **4** (E = S), only displaced by ca. 50 K to higher temperatures. The magnitude of the increase is also significantly reduced compared to **4**, in which the susceptibility surges to a maximum value near 800×10^{-6} emu mol^{-1} at 500 K, before decomposition and loss of magnetization set in. We interpret the very slight hysteretic behavior over repeated cycles over the temperature range 400–600 K as before, in terms of the generation of phase kinks in the lattice, but the reduced magnitude of the effect suggests a more rigid structure.

Accurate single-crystal conductivity measurements on **5** over a broad temperature range were hampered by the limited size and low conductivity of the crystals. The best of several samples examined afforded a room-temperature conductivity near 10^{-7} S cm^{-1}, a value which rose to near 10^{-4} S cm^{-1} near 600 K. Although these data have only qualitative significance, comparison of the room-temperature conductivities of **5** and **4** (E = S) indicates an enhanced conductivity for the triradical system, an observation in keeping with the closer intrastack S···S contacts described above and the band structure calculations described below.

Band Structure Calculations. Extended Hückel band structure calculations, employing the parameters described previously, have been performed on both a single one-dimensional stack of triradicals and also the full three-dimensional lattice. The former affords a direct comparison with similar calculations on **4** (E = S), while the latter allows some measure of interstack interactions. The results are presented in the form of density of states diagrams (Figure 7) and band dispersion curves parallel to a^* which, given

Table II. Bond Lengths and Angles in 1,3,5-$C_6H_3(CN_2S_2)_3$ (**5**)[a]

Bond Lengths (Å)			
S(1)–S(2)	2.082 (3)	N(7)–C(4)	1.349 (10)
S(1)–N(1)	1.619 (7)	N(8)–C(4)	1.321 (9)
S(2)–N(2)	1.630 (6)	N(9)–C(5)	1.347 (9)
S(3)–S(4)	2.075 (3)	N(10)–C(5)	1.346 (9)
S(3)–N(3)	1.637 (6)	N(11)–C(6)	1.311 (10)
S(4)–N(4)	1.650 (6)	N(12)–C(6)	1.342 (10)
S(5)–S(6)	2.098 (3)	C(1)–C(7)	1.479 (10)
S(5)–N(5)	1.641 (6)	C(2)–C(9)	1.489 (10)
S(6)–N(6)	1.627 (6)	C(3)–C(11)	1.478 (10)
S(7)–S(8)	2.084 (3)	C(4)–C(13)	1.490 (9)
S(7)–N(7)	1.625 (6)	C(5)–C(15)	1.472 (10)
S(8)–N(8)	1.633 (6)	C(6)–C(17)	1.477 (10)
S(9)–S(10)	2.073 (3)	C(7)–C(8)	1.398 (10)
S(9)–N(9)	1.620 (6)	C(7)–C(12)	1.377 (10)
S(10)–N(10)	1.627 (6)	C(8)–C(9)	1.384 (10)
S(11)–S(12)	2.100 (3)	C(9)–C(10)	1.380 (10)
S(11)–N(11)	1.640 (6)	C(10)–C(11)	1.407 (10)
S(12)–N(12)	1.626 (6)	C(11)–C(12)	1.374 (10)
N(1)–C(1)	1.354 (9)	C(13)–C(14)	1.368 (10)
N(2)–C(1)	1.355 (9)	C(13)–C(18)	1.392 (10)
N(3)–C(2)	1.331 (9)	C(14)–C(15)	1.390 (10)
N(4)–C(2)	1.343 (9)	C(15)–C(16)	1.380 (10)
N(5)–C(3)	1.328 (9)	C(16)–C(17)	1.385 (10)
N(6)–C(3)	1.332 (10)	C(17)–C(18)	1.383 (10)

Bond Angles (deg)			
S(2)–S(1)–N(1)	95.31 (25)	N(7)–C(4)–N(8)	123.3 (6)
S(1)–S(2)–N(2)	94.86 (24)	N(7)–C(4)–C(13)	117.8 (6)
S(4)–S(3)–N(3)	95.06 (24)	N(8)–C(4)–C(13)	118.8 (6)
S(3)–S(4)–N(4)	94.67 (23)	N(9)–C(5)–N(10)	121.7 (6)
S(6)–S(5)–N(5)	95.02 (24)	N(9)–C(5)–C(15)	119.4 (6)
S(5)–S(6)–N(6)	93.7 (3)	N(10)–C(5)–C(15)	118.9 (6)
S(8)–S(7)–N(7)	94.8 (3)	N(11)–C(6)–N(12)	123.0 (6)
S(7)–S(8)–N(8)	94.63 (24)	N(11)–C(6)–C(17)	119.4 (6)
S(10)–S(9)–N(9)	95.06 (23)	N(12)–C(6)–C(17)	117.7 (6)
S(9)–S(10)–N(10)	94.79 (23)	C(1)–C(7)–C(8)	121.8 (6)
S(12)–S(11)–N(11)	94.6 (3)	C(1)–C(7)–C(12)	118.9 (6)
S(11)–S(12)–N(12)	93.5 (3)	C(8)–C(7)–C(12)	119.2 (6)
S(1)–N(1)–C(1)	113.9 (5)	C(7)–C(8)–C(9)	119.5 (6)
S(2)–N(2)–C(1)	113.8 (5)	C(2)–C(9)–C(8)	120.5 (6)
S(3)–N(3)–C(2)	113.7 (5)	C(2)–C(9)–C(10)	118.5 (6)
S(4)–N(4)–C(2)	113.2 (5)	C(8)–C(9)–C(10)	121.0 (7)
S(5)–N(5)–C(3)	112.9 (5)	C(9)–C(10)–C(11)	119.4 (6)
S(6)–N(6)–C(3)	114.6 (5)	C(3)–C(11)–C(10)	120.2 (6)
S(7)–N(7)–C(4)	113.4 (5)	C(3)–C(11)–C(12)	120.7 (6)
S(8)–N(8)–C(4)	113.8 (5)	C(10)–C(11)–C(12)	119.1 (6)
S(9)–N(9)–C(5)	114.2 (5)	C(7)–C(12)–C(11)	121.8 (6)
S(10)–N(10)–C(5)	114.2 (5)	C(4)–C(13)–C(14)	121.7 (6)
S(11)–N(11)–C(6)	114.0 (5)	C(4)–C(13)–C(18)	118.6 (6)
S(12)–N(12)–C(6)	114.9 (5)	C(14)–C(13)–C(18)	119.8 (6)
N(1)–C(1)–N(2)	122.1 (6)	C(13)–C(14)–C(15)	119.8 (6)
N(1)–C(1)–C(7)	117.7 (6)	C(5)–C(15)–C(14)	120.4 (6)
N(2)–C(1)–C(7)	120.2 (6)	C(5)–C(15)–C(16)	119.1 (6)
N(3)–C(2)–N(4)	123.3 (6)	C(14)–C(15)–C(16)	120.4 (6)
N(3)–C(2)–C(9)	119.0 (6)	C(15)–C(16)–C(17)	120.2 (6)
N(4)–C(2)–C(9)	117.6 (6)	C(6)–C(17)–C(16)	121.3 (6)
N(5)–C(3)–N(6)	123.8 (6)	C(6)–C(17)–C(18)	119.8 (6)
N(5)–C(3)–C(11)	118.6 (6)	C(16)–C(17)–C(18)	119.0 (6)
N(6)–C(3)–C(11)	117.5 (6)	C(13)–C(18)–C(17)	120.9 (6)

[a] esd's are in parentheses.

that $\beta = 99.8°$, approximates the stacking direction in real space. In keeping with the tight intrastack contacts, the density of states diagram for a single column of **5** reveals a smaller band gap (0.8 eV) than is observed (1.4 eV) for a single column of **4** (E = S). The inclusion of interstack contacts in **5** leads to a further decrease of 0.1 eV.

Analysis of the band dispersion diagrams in Figure 8 provides an interesting insight into the effect of the extent of intrastack interactions present in **5** compared to **4**. To interpret the data it is necessary to recall the origins, within a molecular orbital context, of band dispersion. At the simplest (HMO) level of theory, both the dispersion and separation of the valence and conduction bands of a one-dimensional stack of alternate long and short contacts can be described in terms of the two resonance integrals β_1 and β_2 ($|\beta_1| > |\beta_2|$). Accordingly, as the alternating

Table III. Intra- and Interstack Contacts[a] (Å) in 1,3,5-$[C_6H_3(CN_2S_2)_3]$ (**5**) (See Figures 2–5)

Intrastack Contacts					
A		B		C	
S5···S11′	3.758 (3)	S3···S9	3.888 (3)	S1···S7′	3.819 (3)
S5···S11	3.201 (3)	S3···S9′	3.050 (3)	S1···S7	3.131 (3)
S6···S12′	3.876 (3)	S4···S10	3.805 (3)	S2···S8′	3.846 (3)
S6···S12	3.082 (3)	S4···S10′	3.135 (3)	S2···S8	3.104 (3)

Interstack Contacts			
A		B/C	
S5···S5′	3.340 (5)	S1···S4′	3.373 (3)
S5···S6′	3.633 (3)	S1···S4″	4.354 (3)
S5···S11′	3.333 (3)	S1···S10′	3.784 (3)
S5···S12′	3.623 (3)	S1···S10″	3.503 (3)
S6···S11′	3.688 (3)	S7···S4′	3.681 (3)
S11···S11′	3.500 (4)	S7···S4″	3.465 (3)
S11···S12′	3.457 (3)	S7···S10′	3.421 (3)
		S7···S10″	3.724 (3)

[a] Distances within a formula unit are denoted by S···S, those between formula units are designated S···S′ (and S···S″).

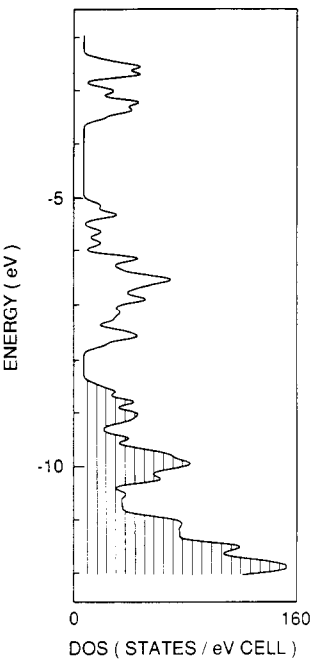

Figure 7. Calculated density of states of **5**.

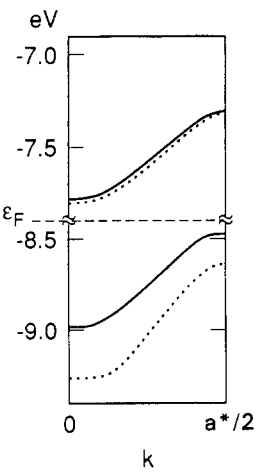

Figure 8. One-dimensional dispersion curves for the valence and conduction bands of **5**. The solid line refers to the full three-dimensional structure, while the dashed line refers to a single column of triradicals.

intrastack contacts (and hence β_1 and β_2) more nearly approach one another, both the valence and conduction bands spread until the two coalesce at $\beta_1 = \beta_2$. In the EHMO model used here, however, where overlap is explictly included, band dispersion is concentrated preferentially in the conduction (antibonding) band. The increase in the conduction band dispersion on passing from single 1-D stacks of **4** (E = S) to those of **5** (0.3 to 0.5 eV) is larger than for the corresponding increase (0.4 to 0.5 eV) observed for the valence bands of **4** and **5**.

Perhaps surprisingly, in view of the number and magnitude of interstack contacts described above, dispersion along b^* and c^*, i.e., approximately perpendicular to the stacking axis, is negligible. This absence of 3-D interactions is also apparent in α-**4** (E = S), although it should be noted that in the case of α-**4** (E = Se) the closer interstack interactions, coupled with the larger selenium radius, lead to substantial band spreading.

Discussion

The 1,3,5-benzene-based tris(dithiadiazolyl) triradical **5** represents the most tightly packed of the stacked dithiadiazolyl structures reported to date. The mode of association up and down the stacks, in which two radical rings per molecular unit bind "up" and the third binds "down", represents an extension of the simple zigzag stacking found in α-**4**. The present structure is, however, considerably more thermally stable. This structural stability is also manifested in the higher temperatures required to induce radical uncoupling and the lowered susceptibility toward hysteretic magnetic behavior (phase kinks) at elevated temperatures. The compression of the stacks, represented by the shortened interdimer S···S contacts, leads to small but real increases in the dispersion of both the valence and conduction bands and a consequent decrease in the calculated band gap. The conductivity of **5** is low and the mechanism of conduction is still open to question, but we note that NMR measurements on α-**4** militate against a mechanism involving phase kink migration.[11] To the extent that conduction can be attributed to thermal excitation across the band gap, the 2 orders of magnitude increase in conductivity between α-**4** (E = S) and **5** can be related to the calculated decrease in band gap.

The results obtained from the polyfunctional dithia- and diselenadiazolyl structures we have studied suggest that the formation of stacked columns is associated with the clustering of four radicals in a pinwheel arrangement. In order to increase the magnitude of intercolumnar interactions, and hence band dispersion, it may be useful to focus on modifying known molecular systems in a manner which enhances contacts while maintaining the pinwheellike solid-state motif. Experiments to this end are currently in progress.

Experimental Section

Starting Materials and General Procedures. 1,3,5-Benzenetricarbonyl trichloride, lithium bis(trimethylsilyl)amide, sulfur dichloride, and triphenylantimony were all obtained commercially (Aldrich). Sulfur dichloride was distilled before use, and $LiN(SiMe_3)_2$ was converted into its diethyl etherate in order to facilitate amidine synthesis.[12] Acetonitrile (Fisher HPLC grade) was purified by distillation from P_2O_5. 1,3,5-Tricyanobenzene was prepared by standard literature methods.[13] All reactions were performed under an atmosphere of nitrogen. Mass spectra were recorded on a Kratos MS890 mass spectrometer. ^1H NMR spectra were recorded at 200 MHz on a Varian Gemini 200 spectrometer. Infrared spectra (CsI optics, Nujol mulls) were obtained on a Nicolet 20SX/C FTIR instrument. Elemental analyses were performed by MHW laboratories, Phoenix, AZ.

Preparation of 1,3,5-Benzenetris[*N*,*N*,*N*'-tris(trimethylsilyl)carboxamidine] (6). $LiN(SiMe_3)_2 \cdot Et_2O$ (48.1 g, 200 mmol) was added, as a dry solid, to a slurry of 1,3,5-tricyanobenzene (7.6 g, 50 mmol) in 250 mL of toluene, and the mixture was heated at gentle reflux overnight. Trimethylsilyl chloride (25.0 g, 230 mmol) was added, and the mixture was heated at reflux for an additional 16 h. The mixture was then filtered to remove LiCl, and the filtrate was concentrated to about half its original volume. Upon cooling to room temperature, a white precipitate of 1,3,5-benzenetris[*N*,*N*,*N*'-tris(trimethylsilyl)carboxamidine] (**6**) was formed. The crude product was collected by filtration, washed with CH_3CN, and dried in vacuo. Recrystallization from toluene/CH_3CN (3:1) afforded colorless needles (14.7 g, yield 35%): mp 132–35 °C; ^1H NMR (δ, $CDCl_3$) 0.13 (Me_3Si, 27 H), 7.67 (s, aromatic, 3 H). Anal. Calcd for $C_{36}H_{84}N_6Si_9$: C, 50.64; H, 9.92; N, 9.84. Found: C, 50.67; H, 9.70; N, 10.08.

Preparation of 1,3,5-$C_6H_3(CN_2S_2)_3$ 5. Excess (5 mL) sulfur dichloride in 10 mL of CH_3CN was added to a slurry of **6** (4.26 g, 5.0 mmol) in 100 mL of CH_3CN, and the resulting orange slurry was heated at reflux for 16 h. The crude tris(dithiadiazolium) salt, $[1,3,5\text{-}C_6H_3(CN_2S_2)_3]Cl_3$, so produced was filtered, washed with CH_3CN, and pumped dry in vacuo. This trichloride salt was reduced by treatment with excess Ph_3Sb (3.0 g, 8.5 mmol) in refluxing CH_3CN for 48 h. The black precipitate of crude tris(1,2,3,5-dithiadiazolyl) $[1,3,5\text{-}C_6H_3(CN_2S_2)_3]$ **5** was filtered off, dried in vacuo and purified by sublimation at 270 °C/10^{-2} Torr as small metallic grey needles (0.70 g, yield 40%), decomposed >350 °C. Larger crystals suitable for X-ray work were obtained by sealed-tube sublimation at 290 °C. The material is completely insoluble in all organic media: mass spectrum (EI, *m/e*) 387 (M^+, 15), 309 ([M − S_2N^+], 60), 231 ([M − 2(S_2N^+)], 85), 153 ([M − 3(S_2N^+)], 85), 78 (S_2N^+, 70), 64 (S_2^+, 100); IR (1600–250 cm^{-1}) 1331 (vs), 1170 (w), 980 (w), 906 (w), 836 (w, br), 806 (m), 781 (s), 779 (s), 708 (w), 684 (m), 633 (w), 505 (m), 415 (w) cm^{-1}. Anal. Calcd for $C_9H_3N_6S_6$: C, 27.89; H, 0.78; N, 21.69. Found: C, 28.03; H, 0.93; N, 21.89.

X-ray Measurements. All X-ray data were collected on an ENRAF-Nonius CAD-4 diffractometer at 293 K with monochromated Mo Kα (λ = 0.71073 Å) radiation. Crystals were mounted on glass fibers with epoxy. The cell dimensions were obtained from 25 reflections measured with 2θ in the range 16–18°. The crystals are monoclinic, space group $P2_1/c$, with M = 387.52, a = 6.927 (2), b = 19.798 (3), c = 19.393 (3) Å, β = 99.80 (2)°, V = 1565.64, and Z = 8. Data were collected using a $\theta/2\theta$ technique. The structure was solved using direct methods and refined by full-matrix least-squares, which minimized $\sum w(\Delta F)^2$; the final R and R_w values were 0.055 and 0.067, respectively. Data collection, structure solution, and refinement parameters for both structures are available as supplementary material.

Magnetic Measurements. The magnetic susceptibility was measured from 4.2 to about 650 K by using the Faraday technique. Details of the apparatus have been previously described.[14]

Conductivity Measurements. Single-crystal measurements were made along the long (*a*) axis of the crystals, using silver epoxy to attach the leads. Four-point measurements were made in an argon atmosphere, using a Keithley 236 unit.

Band Structure Calculations. The band structure calculations were carried out with the EHMACC suite of programs using the parameters discussed previously.[6,15] The off-diagonal elements of the Hamiltonian matrix were calculated with the standard weighting formula.[16]

Acknowledgment. Financial support at Guelph was provided by the Natural Sciences and Engineering Research Council of Canada and at Arkansas by the National Science Foundation (EPSCOR program).

Registry No. 5, 141171-70-2; **6**, 141171-71-3; $LiN(SiMe_3)_2$, 4039-32-1; Me_3SiCl, 75-77-4; 1,3,5-tricyanobenzene, 10365-94-3.

Supplementary Material Available: Tables of crystal data, structure solution and refinement (S1), and anisotropic thermal parameters (S2) for the title compound **5** (4 pages). Ordering information is given on any current masthead page.

(11) Allen, L. C.; Warren, W. W.; Haddon, R. C.; Oakley, R. T.; Cordes, A. W. *Phys. Rev. B* **1991**, *43*, 11456.
(12) Boerê, R. T.; Oakley, R. T.; Reed, R. W. *J. Organomet. Chem.* **1987**, *331*, 161.
(13) Bailey, A. S.; Henn, B. R.; Langdon, J. M. *Tetrahedron* **1963**, *19*, 161.
(14) (a) DiSalvo, F. J.; Waszczak, J. V. *Phys. Rev.* **1981**, *B23*, 457. (b) DiSalvo, F. J.; Waszczak, J. V.; Tauc, J. *Phys. Rev.* **1972**, *B6*, 4574.
(15) Basch, H.; Viste, A.; Gray, H. B. *Theor. Chim. Acta* **1965**, *3*, 458.
(16) Ammeter, J. H.; Burghi, H. B.; Thibeault, J. C.; Hoffmann, R. *J. Am. Chem. Soc.* **1978**, *100*, 3686.